Internal friction measurements of ion beam sputtered amorphous silica

Thomas H. Metcalf,* Xiao Liu,† and Matthew Abernathy‡
US Naval Research Laboratory, Code 7130, Washington, DC 20375, USA

Raymond Robie
NRC Postdoctoral Research Associate at the US Naval Research Laboratory

Massimo Granata, Lorenzo Mereni, Christophe Michel, and Julien Teillon
Laboratoire des Matériaux Avancés – IP2I, CNRS, Université Claude Bernard Lyon 1, 69100 Villeurbanne, France

Gianpietro Gagnoli
Institut Lumière Matière, Université Claude Bernard Lyon 1, CNRS, 69100 Villeurbanne, France

(Received 13 March 2026; accepted 15 July 2026; published 24 August 2026)

The ability to minimize low-temperature acoustic loss in amorphous materials would have implications in fields as wide-ranging as gravitational wave detection and quantum computing. In this paper, we measure the internal friction between 300 mK and room temperature of several thin silica films deposited by ion beam sputtering onto ultra-high-Q silicon resonators. The measurements reveal internal configurations of as-deposited films that are markedly different from that of bulk silica. Over a broad temperature range, the films' internal frictions differ from one another by a factor of two; by contrast, a review shows that sub-MHz internal friction measurements of bulk silica fall within a 35% band with a pronounced main absorption peak between 20 K and 40 K. This peak is absent in the films presented here, except for one film that had been annealed at 900 °C. Annealing at 500 °C erased the thermal histories of the other thin films to create internal friction values that are consistent from film-to-film but yet still markedly different from those of the bulk below 100 K, while creating the steep bulk-like drop-off above 100 K that the as-deposited films lacked. In the context of theoretical structural modeling, our results suggest that exposure to temperatures of at least 900 °C is needed to form the network of tetrahedra considered characteristic of amorphous silica. The present measurements, especially when compared alongside previous work, appear to show that these structures are suppressed in many thin film preparations. These measurements also show, for as-deposited films, an excess of excitations in the 0.15–0.3 eV range which can be annealed away to bring about the Q^{-1} drop-off above the main absorption peak. The shear moduli of all the films are qualitatively similar to bulk silica, with a positive temperature coefficient above a minimum near 60 K and a negative temperature coefficient below.

DOI: 10.1103/hsgl-xhng

I. INTRODUCTION

While it is well recognized that the physical properties of glasses depend upon the conditions of their creation, principally the cooling rate, two recent phenomena illustrate the particularly large degree of variation made possible by vapor deposition. First, at low temperatures, between ∼1 K and 10 K, glassy materials are known to have a population of low-energy excitations that gives rise to an internal friction between $10^{-4} \leqslant Q^{-1} \leqslant 10^{-3}$, regardless of chemical composition or bonding [1]; however, vapor-deposited amorphous silicon has been measured as low as $Q^{-1} \leqslant 2 \times 10^{-6}$ [2,3]. Second, vapor deposited organic glasses have achieved densities that, if cooled from a melt, would take on the order of 1000 years of annealing to achieve [4,5]. In both of these examples, vapor deposition has enabled the large deviation from bulk behavior.

In this paper, we seek to understand the range of properties in thin films of vapor-deposited amorphous SiO_2—perhaps the prototypical glass—through measurements of internal friction and shear modulus. A consideration of relaxation barrier heights allows us to consider our results in the context of 70 years of theoretical structural modeling of amorphous silica. The low-energy excitations, which have been observed in all amorphous solids except the aforementioned amorphous silicon, have been successfully modeled as a broad distribution of two-level tunneling systems (TLSs) [6,7], the spectral density of which can be directly measured through internal friction. Discovering the conditions under which the density of TLSs in a material system can be substantially reduced would be of tremendous practical interest, as TLSs can couple to the quantum state of superconducting qubits, causing unwanted decoherence [8]. Thin silica coatings also serve as the low-refractive-index material in the alternate-layer

*Contact author: thomas.h.metcalf.civ@us.navy.mil
†Retired.
‡Present address: The Johns Hopkins University Applied Physics Laboratory, Laurel, Maryland 20723, USA.

TABLE I. Deposition and measurement summary of films reported on in this paper, as-deposited (AD), after annealing (Ann), and change upon annealing. Both GC-2 and GC-2b were annealed before measurement. S-3b was deposited after S-3 measurements were completed. Except for S-GeNS, the Q_0^{-1} is the low-temperature internal friction plateau value discussed in Sec. VII and the change in shear modulus value ΔG_{film} is the value for $T < 1$ K, discussed in Sec. IX. The S-GeNS datum is for $T = 115$ K. Annealing was conducted in air.

Film	t_{film} (nm)	AD $Q_0^{-1}\times10^{-4}$	Temp. (°C)	Ann $Q_0^{-1}\times10^{-4}$	$\Delta Q_0^{-1}\times10^{-4}$	ΔG_{film} (GPa)
			Grand Coater films			
GC-1	210	10.4	500	6.0	–4.4	1.9
GC-2	339		900	5.2		
GC-2b	+344					
			SPECTOR films			
S-1	196	5.7	500	6.8	1.1	–0.4
S-2	194	5.0	500	7.4	2.3	–0.4
S-3	690	3.8	500	5.5	1.7	–0.2
S-3b	+860		500	5.4		
S-GeNS	194	3.4				

sandwich structure of the Bragg reflectors in gravitational-wave interferometers [9]. The sensitivity-limiting thermal noise from the coating layers is directly related to its internal friction, and a reduction in coating internal friction is a primary avenue for improved sensitivity of future detectors.

II. FILMS

The thin film samples studied in this work were deposited in two different ion-beam sputtering (IBS) coating facilities at the Laboratoire des Matériaux Avances (LMA) onto high-quality factor (Q) mechanical resonators. We used a commercial Veeco SPECTOR system and a large, custom-developed facility (called *Grand Coater*, GC) that is used to deposit the current mirror coatings for the Advanced LIGO, Advanced Virgo, and KAGRA gravitational-wave interferometers. Accelerated argon ions were used as sputtering particles while oxygen was injected into the deposition chambers, for a total working pressure of the order of 10^{-4} mbar. In the SPECTOR, the beam voltage and current were 1.3 kV and 0.6 A, respectively, yielding an average growth rate of 0.24 nm/s, while the substrates were heated to ∼150 °C. Similar conditions were used in the GC, which uses a proprietary process designed to optimize film optical properties. Each film for this experiment, except for S-GeNS, was deposited onto an individual double-paddle-oscillator (DPO) resonator, while S-GeNS was deposited onto a silicon wafer for use in a clamp-free Gentle Nodal Suspension (GeNS) system [10] adapted for cryogenic measurements [11]. Film thicknesses were measured by fits of transmission photometric spectra of witness samples deposited onto SF11 glass substrates. All the films are summarized in Table I. Further physical properties of similar GC and SPECTOR-grown silica films can be found in Ref. [9].

The films S-1, S-2, GC-1, and S-GeNS are all ≈200 nm thick. The film S-GeNS was codeposited in the SPECTOR together with S-2. Except for GC-2, samples were initially measured as deposited, then the film-laden resonators were subsequently annealed in air to 500 °C for 36 ks, after which they were measured again. The film S-3, ≈700 nm-thick, was originally a test deposition, but was used in a separate experiment to determine whether the curvature of the DPO resulting from the film strain had a significant effect on the internal friction measurements, as detailed in Sec. IV. For this measurement, the film S-3b was deposited onto the other side of the DPO after the film S-3 had been measured and annealed.

For GC-2, silica films were deposited on both surfaces of the DPO, after which the DPO was annealed in air at 900 °C for 36 ks, with 32 ks temperature ramps up and down.

III. RESONATOR MEASUREMENTS

The outline of a DPO, representing its top surface, is shown in Fig. 1(a). The DPO is fabricated from [100]-oriented single-crystal silicon wafers using standard microfabrication techniques [12]. Both the top and bottom surfaces of the wafer are coated with 800 Å of silicon nitride grown by low-pressure chemical vapor deposition. The top nitride coating is patterned into the shape of Fig. 1(a), to act as a mask for the release step, an etch in a hot potassium hydroxide solution. This etches the top (100) surface approximately 150 times faster than any {111} surface [13], creating the beveled sidewalls of the DPO and bottom edges that extend outward a further 212 µm.

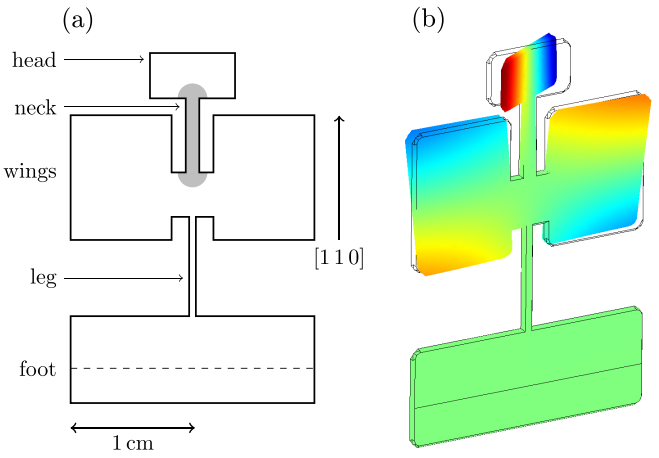

FIG. 1. (a) outline of top surface of DPO resonator with various components labeled. Shaded area represents deposited film. (b) FEM calculation of mode shape of AS2. Color scale reflects out-of-plane deflection.

Exterior corners are composed of {110} and {311} faces [14], which etch at rates comparable to that at which {100} surfaces etch; the longer newly released DPOs are kept in the etch bath, the more material is removed from the corners. A metal film electrode is deposited onto the wings, leg, and foot—but not the neck or head—of the back side of the DPO for capacitive drive and detection. In the case of 900 °C-annealed GC-2, to avoid contamination, the metal film electrode was deposited after annealing. Finally, the bare DPOs are annealed in high vacuum conditions at 450 °C for 10 ks, a step that has been shown to improve the quality factor [12].

The gray zone in Fig. 1, an area of approximately 1.2 mm×7 mm, indicates the "neck" area onto which films were deposited through a shadow mask, generally onto the wider back face of the DPO. The bottom of the foot of the DPO, below the dashed line in Fig. 1(a), is clamped in an Invar sample holder, which is mounted inside the vacuum can of a ^{3}He cryostat that can be cooled to 375 mK.

The GeNS measurement was performed on a 75 mm diameter, 450-μm-thick, [100]-oriented Si wafer. Both DPO and GeNS measurements are conducted by free ringdown decay, where the damping is determined from the $1/e$ decay time τ of a mode at resonant frequency f as $Q^{-1} = (\pi f \tau)^{-1}$.

We excite the ninth resonant mode of the DPO, a torsional mode referred to as the second antisymmetric mode and abbreviated as AS2 [15,16]. A finite element rendering of the mode shape of AS2 is shown in Fig. 1(b): the wings twist about their horizontal axis and the head twists about the neck in a mechanically balanced manner such that there is negligible twisting of the leg, concentrating the strain energy in the neck. The head and wings are 180° out of phase with one another; when one side of the head is moving up, the top of the wing on the same side is moving down. Modeled as a lightly damped harmonic oscillator, the (lumped-element) inertial term is given by the moment of inertia of the head, and the restoring force is given by the torsion constant of the neck. The resonant frequency of AS2 can lie between 5.4 kHz and 7 kHz as the moment of inertia of the head depends strongly on the degree of etching of the corners.

Because of the wide range of AS2 frequencies, the frequency and Q^{-1} of a bare DPO is measured before film deposition, except for GC-2. For GC-2, the bare DPO was measured last, after stripping the silica film from the DPO. To strip the film, the rest of the DPO surfaces were covered with a protective coating [17] and the DPO was immersed in a 25% hydrofluoric acid solution for 300 s. In this way, any changes to the DPO as a result of the annealing process were retained and thus accounted for in the background frequency and quality factor.

For the DPO, in a thin film approximation, changes to the resonant frequency and damping of the resonator upon deposition of a film are given by

$$\frac{f_{\text{film-laden}} - f_{\text{sub}}}{f_{\text{sub}}} = \frac{\Delta f}{f} = \frac{3G_{\text{film}}t_{\text{film}}}{2G_{\text{sub}}t_{\text{sub}}}, \tag{1}$$

$$Q^{-1}_{\text{film-laden}} = \frac{3G_{\text{film}}t_{\text{film}}}{G_{\text{sub}}t_{\text{sub}}}Q^{-1}_{\text{film}} + Q^{-1}_{\text{sub}}, \tag{2}$$

$$= 2\frac{\Delta f}{f}Q^{-1}_{\text{film}} + Q^{-1}_{\text{sub}}, \tag{3}$$

where the G's are shear moduli, t's are thicknesses, "film" refers to the silica film itself and "sub" refers to the bare DPO substrate [18]. We use Δ to represent changes from the deposition of a film or from annealing, and will use δ to represent changes in a resonator as a function of temperature.

The GeNS measurement uses a frequency-dependent dilution factor D [19],

$$D = 1 - \frac{m_{\text{sub}}}{m_{\text{film-laden}}}\left(\frac{f_{\text{sub}}}{f_{\text{film-laden}}}\right)^2, \tag{4}$$

where m_{sub} and $m_{\text{film-laden}}$ are the bare and film-coated wafer masses, respectively, measured for this work with an analytical balance. Then,

$$Q^{-1}_{\text{film}} = \frac{1}{D}\left(Q^{-1}_{\text{film-laden}} + (D-1)Q^{-1}_{\text{sub}}\right). \tag{5}$$

For this work, we measured the resonance at ∼0.6 kHz, which falls within the detection band of ground-based gravitational-wave detectors (∼0.03 − ∼2 kHz). For this mode, $D \approx 1.5 \times 10^{-3}$. More details about this data analysis method can be found elsewhere [9,20].

The DPO measurements and calculations are illustrated in Fig. 2 using film S-1 as an example, with internal friction in panel (a) and frequency in panel (b). The internal friction measurements in Fig. 2(a) are shown both on a log-log scale and, in the inset, on a linear scale. The Q^{-1} of AS2 of a bare resonator is shown as the lowest-lying curve. Despite being primarily a torsional mode, the Q^{-1} of AS2 above 50 K is dominated by thermoelastic loss from residual flexure in the wings [21]. Below 30 K, $Q^{-1}_{\text{sub}} < 2 \times 10^{-8}$. The deposition of a film increases the measured Q^{-1} value, shown by the middle curve, over the entire temperature range by an amount $3 \times 10^{-7} \lesssim \Delta Q^{-1} \lesssim 6 \times 10^{-7}$, which at low temperatures represents an increase by one and a half orders of magnitude. Although at high temperatures Q^{-1}_{sub} and $Q^{-1}_{\text{film-laden}}$ appear to converge on a log scale, the linear scale inset shows a measurable difference.

Figure 2(b) shows the frequencies recorded in the same measurements. In this example, the frequency of the bare DPO rises by $\delta f \approx 29$ Hz between room temperature and low temperature, for $\delta f/f|_{\text{RT-LT}} \approx 4.48 \times 10^{-3}$. To first order, this follows the rise of the shear modulus in silicon G_{Si} as $\delta f/f = \frac{1}{2}\delta G_{\text{Si}}/G_{\text{Si}}$. The addition of this film causes an increase in the frequency of approximately $\Delta f = 3.1$ Hz, for $\Delta f/f \approx 4.8 \times 10^{-4}$. The inset to Fig. 2(b) shows that the low-temperature variation is much stronger for the film-laden DPO than for the bare DPO; the scaling of the y axis is the same for both sections of the inset. For the bare DPO, the relative frequency variation is $\delta f/f \leqslant 2 \times 10^{-9}$ below 2 K, and drops by $\delta f/f \approx 10^{-7}$ between base temperature and 10 K, while the film-laden DPO has a variation $\delta f/f \leqslant 2 \times 10^{-7}$ below 2 K and drops by $\delta f/f \approx 2 \times 10^{-6}$ between base temperature and 10 K.

By inverting Eq. (2), we can extract the internal friction of the film itself, Q^{-1}_{film}, represented in the top-most curve (not shown in linear scaling). Likewise, if the film thickness t_{film} is known, then the film shear modulus G_{film} can be calculated via Eq. (1). In these calculations, Q^{-1}_{sub}, $Q^{-1}_{\text{film-laden}}$, f_{sub}, and $f_{\text{film-laden}}$ are all functions of temperature, while t_{sub}, t_{film}, and G_{sub} are considered fixed values. Note that the Q^{-1}_{film}

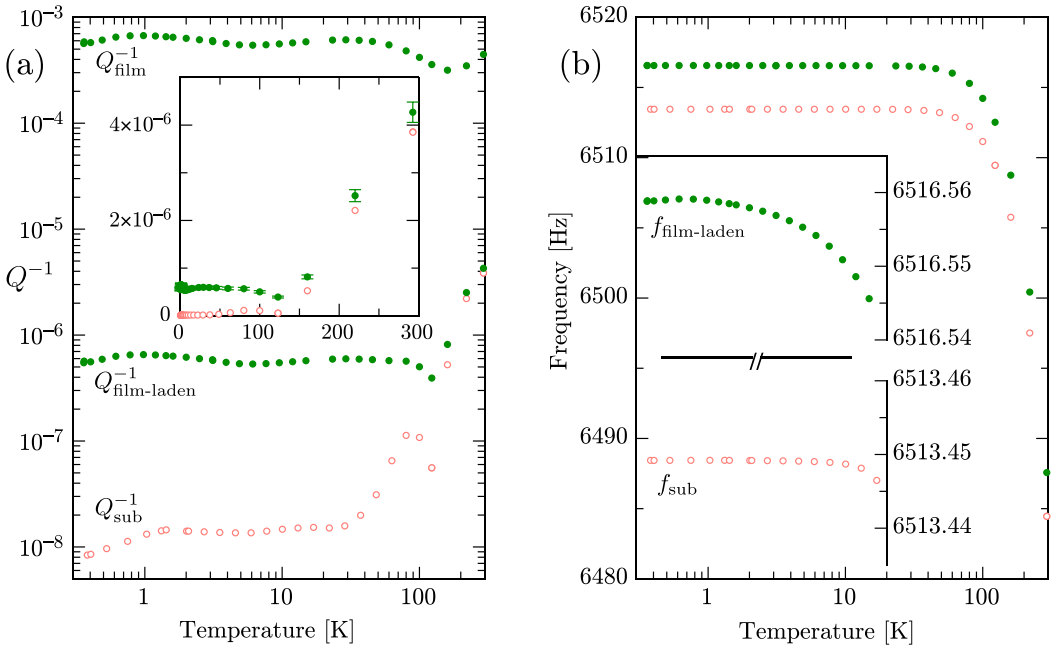

FIG. 2. (a) Q^{-1} values throughout measurement and analysis for as-deposited film S-1. Inset shows same Q^{-1}_{sub} and $Q^{-1}_{\text{film-laden}}$ data on linear scale. Error bars on the inset represent 5% of the Q^{-1} value and would be smaller or comparable for Q^{-1}_{sub}. (b) Frequencies for bare and as-deposited S-1. Inset uses same x-axis temperature scale as main figure and both segments of inset use the same y-axis scaling on the right.

calculation does not depend on precise knowledge of either G_{film} or t_{film}; their product appears in both the frequency shift and the energy loss scaling of Eq. (2).

To verify that the postannealing measurements primarily reflect changes to the film and not the underlying substrate, a bare, measured DPO was put through the same annealing procedure as the films and measured again before film deposition. At 500 °C, we do not expect significant thermal growth of silica; an extrapolation of the thermal silica growth rates measured by Deal predicts well under a nanometer of growth [22]. The annealed bare DPO did show an increase of background damping $\Delta Q^{-1} \approx 7 \times 10^{-9} \ll Q^{-1}_{\text{film-laden}}$, which would change the Q^{-1}_{film} calculation by $\backsim 1\%$, an amount smaller than the error bars shown. Because the effect of the annealing on the part of the substrate covered by the film is unknown, we did not try to apply a correction to Q^{-1}_{sub} of the annealed films.

IV. CURVATURE

The deposition of the film on only one side of the DPO introduces a stress asymmetry. As the film S-3 was more than three times thicker than the other films, any effect of this asymmetry on the internal friction ought to be the most pronounced in this film. To determine its effect on the measurement, a second film, S-3b, was deposited on the opposite side of the DPO. Because S-3 was deposited on the wider back of the DPO, in the neck region, the deposition of S-3b on the narrower top of the DPO was thicker, to bring the total stress into balance. With a film on only one side, the DPO's radius of curvature from the film stress was −6 m, and when the second film was deposited, this flattened to a radius of +38 m. In Fig. 3, both $Q^{-1}_{\text{film-laden}}$ and Q^{-1}_{film} are shown for as-deposited S-3 by solid blue squares and for the annealed film by open blue squares. Because Q^{-1}_{film} post-annealing is measurably higher than before annealing, and because the annealed film was already present on the DPO, S-3b was also annealed (and therefore, S-3 was doubly

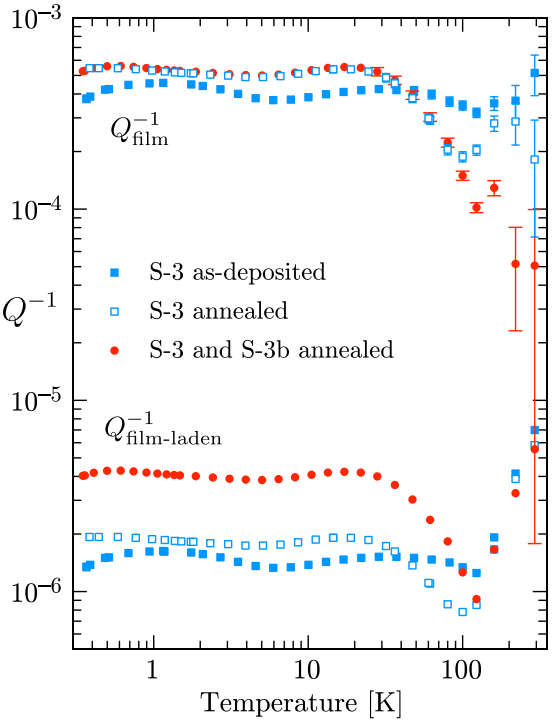

FIG. 3. Measured and calculated Q^{-1} values for S-3 and S-3b: as-deposited single-sided film, solid blue squares; annealed single-sided film, open squares; double-sided annealed film S-3 with S-3b, red circles.

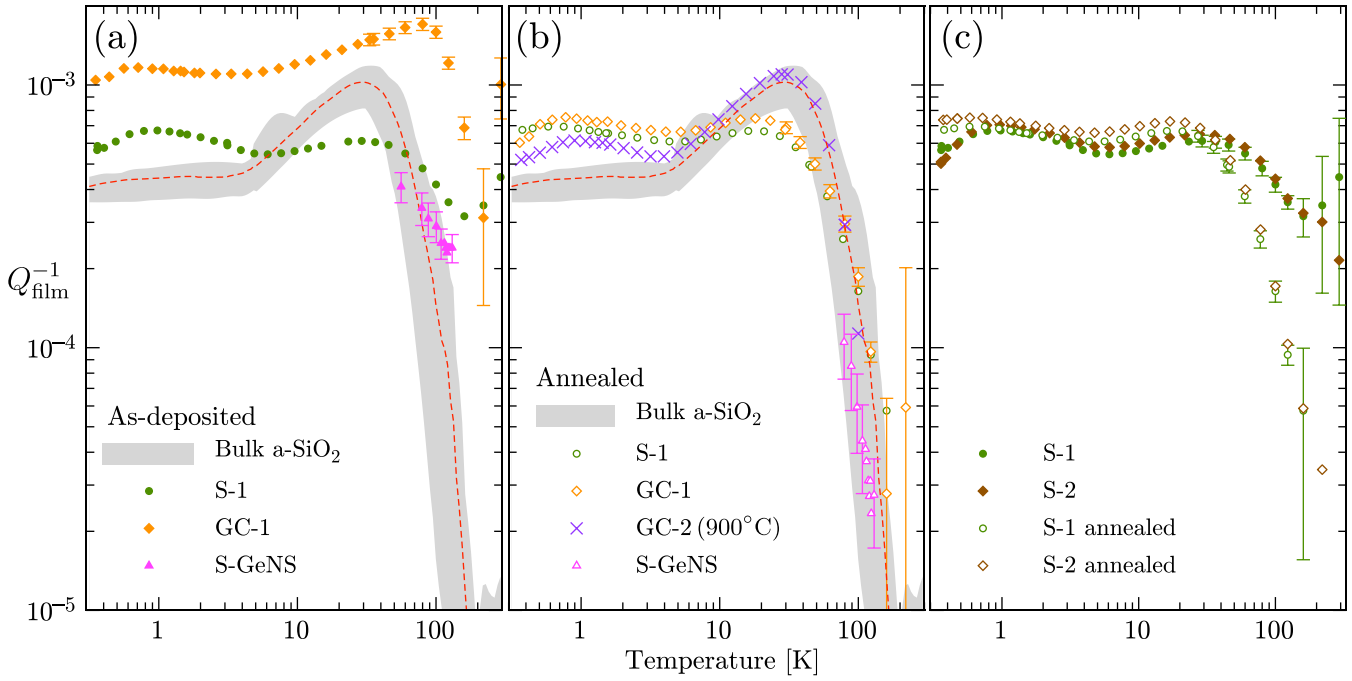

FIG. 4. Calculated internal friction of films in this work. (a) as-deposited; (b) annealed. (c) Comparison of S-1 and S-2 in both as-deposited and annealed state. Closed symbols: as-deposited; open symbols, annealed. Gray band in (a) and (b) represents range of internal friction values found in literature for bulk silica measured at frequencies less than 1 MHz, the red dashed line is their mean; see text for specific references. For clarity, only select error bars are shown; those at 30 K are representative of those at lower temperatures. Error bars for GC-2, a thicker sample, are approximately the size of the symbols.

annealed) before measurement. With two films contributing to the mechanical loss, $Q^{-1}_{\text{film-laden}}$ increases, as Eq. (2) predicts. These measurements of S-3 and S-3b together are represented by the red closed circles in Fig. 3. Notably, using the sum of the thicknesses of S-3 and S-3b for t_{film}, Q^{-1}_{film} calculations exactly match that of the annealed single-layer film. If the curvature induced by the single-layer film had contributed an additional loss mechanism that the uncurving ameliorated, the Q^{-1}_{film} calculation of the double film would be expected to be lower, reflecting the absence of such a mechanism. As the two calculations give the same results, we conclude that the curvature does not introduce any such mechanism.

Incidentally, while Q^{-1}_{film} of S-3 both as-deposited and annealed follow qualitatively the temperature dependence of S-1 and S-2, the values themselves are lower across the whole temperature range, suggesting a thickness dependence to Q^{-1}_{film}. Although a systematic investigation of thickness dependence is beyond the scope of the present manuscript, it is a subject for further work.

V. INTERNAL FRICTION AND ANNEALING

Internal friction measurements of our films are compared to one another, and to that of bulk silica, in Fig. 4. The internal friction of bulk, fused silica is indicated by the gray band and dashed red line in Figs. 4(a) and 4(b). The band represents the maximum and minimum extent of 21 separate measurement data sets, all for measurement frequencies less than 1 MHz, reported in eleven publications [23–33], with the red dashed line representing their mean. There are three features common to the measurements: First, all measurements show a peak in which the internal friction has a maximum of $\approx 10^{-3}$, often referred to as the "main absorption peak" [34]; this will be discussed in more detail in Sec. VIII. Second, Q^{-1} falls off sharply by more than one order of magnitude at temperatures above the main absorption peak. Third, below the main absorption peak, Q^{-1} settles to a temperature-independent plateau value, $Q_0^{-1} \approx 4 \times 10^{-4}$; this will be discussed in Sec. VII. Amongst the different measurements, the spread of the Q_0^{-1} is generally less than 35%. The temperature T_{max} of the maximum of the main absorption peak is related to the measuring frequency ω as $\ln \omega \propto -1/T_{\text{max}}$, a trend that has been observed between 46 Hz [31] and 36 GHz [35], and for the data included here lies between 24 K and 38 K. At frequencies higher than 1 MHz, the internal friction at the peak increases [36], but for the data included here there is no systematic variation of peak height with frequency.

The large difference in internal friction that can result from film preparation in different deposition chambers is illustrated in Fig. 4(a), which shows the calculated film internal frictions Q^{-1}_{film} of S-1, GC-1, and S-GeNS, all ≈200 nm-thick. Although the depositions nominally use similar film growth parameters, the films' internal friction values are both different from one another, and from the bulk values, over the entire temperature range measured. Near 2 K, the internal friction of GC-1 is 70% higher than that of S-1 and the difference is larger at higher temperatures. Over the temperature range for which GeNS measurements were taken, the GeNS data follow a similar temperature dependence to S-1 but is 30% lower through the thermoelastic minimum at 123 K [37].

When the films undergo 36 ks of annealing in air at 500 °C, the synthesis history that gives rise to their different internal

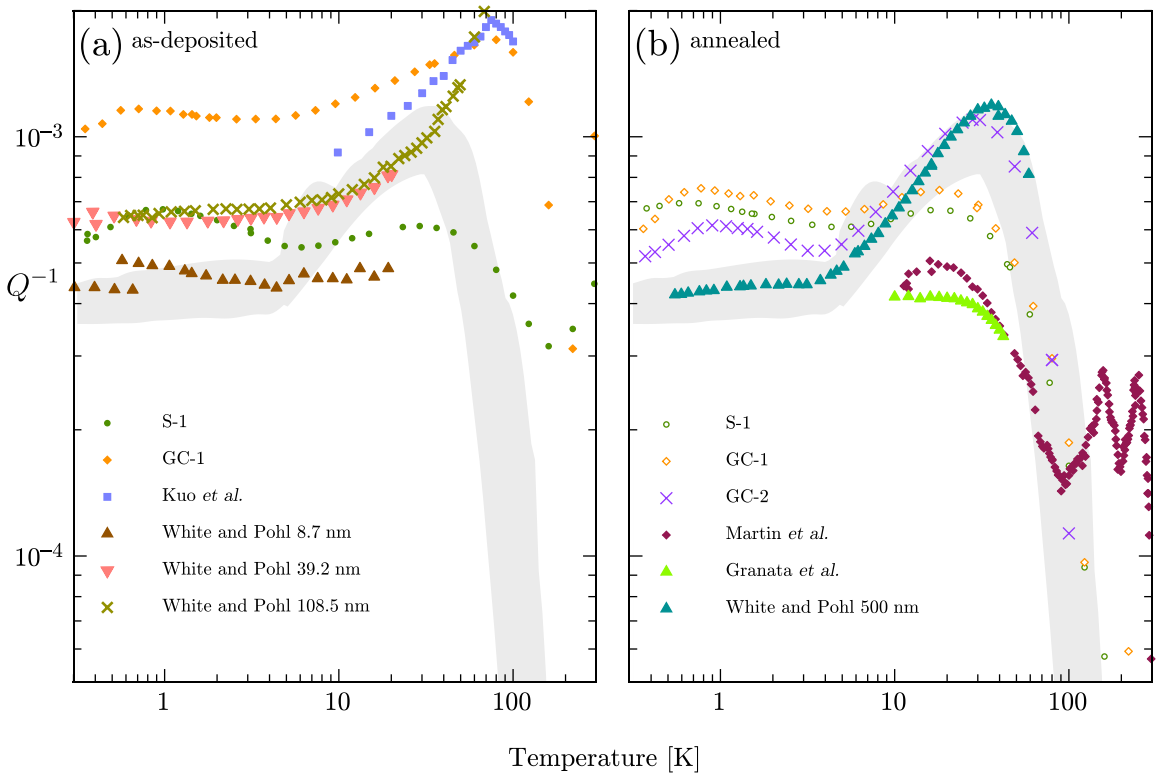

FIG. 5. Internal friction vs temperature for literature thin silica films compared with data presented in this paper. Gray bands represent bulk measurements, as in Fig. 4. (a) Films that were deposited nominally at room temperature and which did not receive a heat treatment; (b) films annealed or deposited at temperatures in excess of 500 °C. Literature film details are in Table II.

friction values is erased and the annealed films are remarkably similar to one another, yet still different than bulk, as is shown in Fig. 4(b). The internal friction of S-1 is slightly higher (by 8%) than before annealing for temperatures less than 30 K, while the internal friction of GC-1 decreases by ∼40% in the same temperature range. The postannealed films have internal frictions within ∼10% of one another. The annealing also creates the high-temperature Q^{-1} drop-off which is characteristic of bulk silica and absent from as-deposited films. This is clearest in the annealed S-GeNS film, but evident in the other films as well. The internal friction for temperatures $T < 10$ K is still higher than for bulk, and there does not appear to be a 30 K peak.

The sample GC-2, annealed at 900 °C, is also shown in Fig. 4(b). In contrast to the 500 °C-annealed films, this film does show a 30 K peak and high-temperature drop-off that in both magnitude and temperature matches that of the bulk samples.

In contrast to the chamber-to-chamber variation seen in Fig. 4(a), Fig. 4(c) shows that films grown in the same deposition chamber to the same thickness with the same parameters—here, S-1 and S-2—do, in fact, have largely identical internal friction measurements. Their internal frictions differ by ∽5% over most of the temperature range. Figure 4(c) also illustrates the subtle, and reproducible, changes to the SPECTOR-grown films after the annealing treatment, after which the films differ by about 8%.

Error bars for $T > 30$ K are shown for GC-1 and S-GeNS in Figs. 4(a) and 4(b) and for S-1 in both as-deposited and annealed in Fig. 4(c). Error bars are calculated using standard propagation of error and are based on a historical, empirical DPO Q^{-1} reproducibility of 5%. Error bars for S-2 are comparable to those for S-1 and for visual clarity are not shown. Error bars for $T < 30$ K are the same as those at 30 K and are ≈5%. The primary source of uncertainty at $T > 30$ K originates from the thermoelastic increase in Q^{-1}_{sub} and the smaller difference between Q^{-1}_{sub} and $Q^{-1}_{\text{film-laden}}$, as can be seen in the inset to Fig. 2.

The as-deposited films shown in Fig. 4(a) differ in several respects from the uniform behavior of bulk silica. The low-temperature plateau value for the films is higher than for the bulk, and they show evidence of a broad and shallow peak centered near 1 K in addition to the low-temperature plateau. None of the films show the main absorption peak, although all show shallower peaks, with the GC-1 peak shifted to 80 K.

Taken together, our measurements reveal several distinct configurations of amorphous silica: a bulk-like configuration achieved with 900 °C annealing, a separate configuration achieved with 500 °C annealing, and at least one other configuration representing the as-deposited films.

VI. COMPARISON WITH OTHER THIN FILM MEASUREMENTS

While bulk silica internal friction measurements are remarkably consistent with one another, we are aware of four published low-temperature studies of thin films of silica, almost all of which show some departure from bulk internal friction. We have compared selected data from these papers to the measurements presented in this paper in Fig. 5, with

TABLE II. Parameters of literature thin films plotted in Figs. 5(a) and 5(b).

Paper	Ref.	t_{film} (nm)	Method	f (kHz)	T (°C)
Kuo *et al.*	[38]	270	IBS	1.9	
White and Pohl	[39,40]	8.7	e-beam	5.5	
White and Pohl	[39,40]	39.2	e-beam	5.5	
White and Pohl	[39,40]	108.5	e-beam	6.3	
White and Pohl	[39,40]	500	thermal	6.3	1025
Martin *et al.*	[41]	1000	IBS	7.3	600
Granata *et al.*	[11]	2500	IBS	5.9	500

as-deposited films in Fig. 5(a) and heat-treated films in Fig. 5(b). A summary of the literature films is presented in Table II.

In the most comprehensive study, White and Pohl used DPO substrates to measure: a 500-nm thermal oxide, 0.75 nm and 109 nm films grown by e-beam evaporation, and an e-beam film originally 2.2 nm-thick and measured after three subsequent deposition steps to eventually reach an accumulated thickness of 39 nm [39,40]. Of White and Pohl's e-beam films, most did not show any sign of the main absorption peak; the 8.7 nm film is shown in Fig. 5(a) as an example. The 39.2 nm film is plausibly consistent with such a peak, although the data cut off at 20 K. The Q^{-1} of White's 108.5 nm film rises with rising temperature, with a peak value $Q^{-1} \geqslant 5 \times 10^{-3}$, well above the bulk main absorption peak, reached at a temperature $T \geqslant 115$ K. White and Pohl's 500 nm thermal oxide film was grown at 1300 K and is shown in Fig. 5(b). This film and GC-2 are the only thin films that clearly show a main absorption peak that aligns with bulk silica, suggesting that exposure to temperatures at or above 900 °C is necessary for the appearance of the main absorption peak.

Aside from White and Pohl's measurements, the other literature thin films were deposited via ion beam sputtering. In these studies, a single film was measured at several frequencies using different modes of the substrate resonator. Internal friction measurements capture all the mechanical energy loss mechanisms that are simultaneously at work, intrinsic as well as extrinsic. In the cases of the Martin *et al.* [41] and Kuo *et al.* [38], the films were deposited on a singly-clamped cantilever: in addition to the internal friction of the silica, each resonant mode will have a different loss associated with cantilever attachment or clamping. It is reasonable, then, to consider the lowest Q^{-1} values as the most representative of the value for the silica film itself: 7307 Hz in the case of Martin *et al.* and 1873 Hz in the case of Kuo *et al.* Granata *et al.* [11] deposited a 2.5-μm film on a silicon wafer for a GeNS measurement, which introduces negligible suspension loss; we chose the 5900 Hz data as it is a close frequency match to our measurements.

Kuo *et al.* deposited a 270-nm film on a nominally room-temperature silicon cantilever and did not perform a heat treatment. This film, shown in Fig. 5(a), shows a high temperature peak very similar to that of GC-1. It is known that argon sputtered silica films can contain on the order of 0.2% argon, which effuses out upon annealing [42]. It is plausible that the peak shown in these two films originates from such included argon in a similar manner as has been observed with 1% hydrogen [43]; the internal friction of argon films rises with temperature [44], increasing sharply near the melting point $T_m = 84.35$ K [45].

The films of Martin *et al.* and Granata *et al.* were heat treated before measurement. Martin *et al.* deposited a 1-μm film at 100 °C on a silicon cantilever, which was subsequently annealed for 24 h at 600 °C, while Granata *et al.*'s film was annealed at 500 °C before measurement. These measurements are shown in Fig. 5(b). Although Martin identifies peaks at 20 K and 160 K, neither exhibits characteristics of the main absorption peak, and Q^{-1}_{film} is notably lower than bulk in the 10–60 K range. Granata *et al.*'s film is similar to Martin *et al.*'s and has slightly lower Q^{-1}_{film}.

Figure 5 is consistent with our measurements: Although bulk silica below 1 MHz shows a stable and consistent internal friction, the mechanical loss in thin film silica is strongly dependent on deposition conditions and annealing. In some instances, as-deposited films can develop strong internal friction peaks near 100 K, which are absent in films annealed near 500 °C.

VII. TWO-LEVEL TUNNELING SYSTEMS

The internal friction of bulk silica below 5 K can be explained via the TLS model. The presence of low-energy excitations in amorphous solids was first observed in measurements of specific heat below 1 K and thermal conductivity below 100 K [46]. The model of these excitations put forth by Anderson, Halperin, and Varma [6] and by Phillips [7] supposed that the amorphous structure creates a potential energy landscape with a population of two-level tunneling systems (TLSs): atoms, or groups of atoms, that have two distinct spatial arrangements with similar energies. Any given TLS could be modeled as an asymmetric double-well potential, with a barrier height V, asymmetry Δ, and separation d, from which a tunnel splitting Δ_0, an energy splitting E, and a tunneling parameter λ can be calculated. At the temperatures of interest, the energy barrier between the wells is too high for thermal activation, but the wavefunction overlap between the two wells, described by λ, is such that the atoms can tunnel between the configurations. To calculate the macroscopic properties, it is presumed that the distribution of the parameters of the two-level systems is uniform: $P(\Delta, \lambda) = \overline{P}\, d\Delta\, d\lambda$.

Jäckle showed that these same two-level systems give rise to two mechanisms of ultrasonic attenuation: resonant and relaxational [47]. Resonant scattering occurs at the lowest temperatures and highest frequencies: A phonon of frequency ν can be absorbed with a TLS with energy splitting E when $E = \hbar\nu$. If $\hbar\nu \ll k_B T$, loss from resonant scattering scales as $Q^{-1}_{\text{res}} \propto \nu/T$, where $\hbar$ is Planck's constant, k_B is the Boltzmann constant, and T is the temperature. At the lowest temperatures of our experiment, $Q^{-1}_{\text{res}} < 10^{-9}$. The data in this paper are relaxational: A strain wave alters the parameters of the TLSs and throws the occupations out of thermal equilibrium, interacting with the phonon bath. At very low temperatures, the relaxational internal friction scales as T^3, but above a crossover temperature T_{co} that depends on the measuring frequency ω as approximately $T_{\text{co}} \approx \sqrt[3]{\omega}/1000$ K for silica (3 mK in DPO measurements), the internal friction levels off to a constant

value,

$$Q_0^{-1} = \frac{\overline{P}\gamma^2}{\rho v^2}, \tag{6}$$

where ρ is the material density, v is the speed of sound, and γ is the phonon coupling constant, calculated as a derivative of Δ with respect to strain.

It is this plateau region with constant Q^{-1} that we see in the bulk silica for $T < 5$ K. The films in this work have an additional shallow peak, centered around 800 mK, on top of a higher TLS plateau, which suggests a larger value of $\overline{P}$ than for bulk silica. An examination of the pre- and postanneal states in Fig. 4(c) shows three distinct regions of changes upon annealing for S-1 and S-2. At the lowest temperatures, below 800 mK, Q_{film}^{-1} rises to create a plateau; at present, we do not have an explanation for this increase. Between the peak and 3 K, the as-deposited and annealed films coincide with one another, suggesting that the annealing does not change $\overline{P}$ and that annealing-related Q^{-1} changes are the result of non-TLS mechanisms. Between 3 K and 30 K, Q_{film}^{-1} is higher in the annealed film; this will be discussed in Sec. VIII.

VIII. MAIN ABSORPTION PEAK

To model the main absorption peak, Gilroy and Phillips [26] (and nearly simultaneously, Vacher *et al.* [48]) took the asymmetric double-well potential of the TLS model and extended it to higher temperatures, with thermally activated jumps between the configurations instead of tunneling. In this regime, the distributions of the parameters of the double well potentials are not constants; instead, the model considered separate distributions $g(V)$ over barrier heights and $f(\Delta)$ over asymmetries. In Gilroy and Phillips's computation, $f(\Delta) = f_0$ was taken to be constant and $g(V) = V_0^{-1} e^{-V/V_0}$ was taken to be exponential. This leads to an internal friction

$$Q^{-1} = \frac{\gamma^2 f_0 \pi k_B T}{M V_0} (\omega\tau_0)^{\frac{k_B T}{V_0}}, \tag{7}$$

where M is the appropriate elastic modulus, V_0 is a parameter from the distribution $g(V)$, and τ_0 is a characteristic time scale for TLS relaxation, which is taken to be $\tau_0 = 10^{-13}$ s. This calculation does fit the main absorption peak of Gilroy and Phillips's 660 kHz measurements on silica (which are among those contributing to the bulk data of Fig. 4). Much subsequent work has been devoted to improved distribution functions and better descriptions of the double well [33,35,49,50].

A further computation in Gilroy and Phillips's model, outlined by Topp and Cahill [51], is to convert the high-temperature Q^{-1} measurements into a barrier height distribution $g(V)$ via

$$g(V) f_0 = \frac{M}{\pi \gamma^2 k_B} \frac{Q^{-1}(T)}{T} \tag{8}$$

and

$$V = -k_B T \ln(\omega\tau_0). \tag{9}$$

This transformation allows a frequency-independent comparison of internal friction measurements, and also allows comparison to energy scales in computational models, as will be discussed in Sec. X. The transformation of the data in Fig. 4 via Eqs. (8) and (9) is shown in Fig. 6. A discussion of the values of γ and the elastic moduli used in these calculations is in the Appendix.

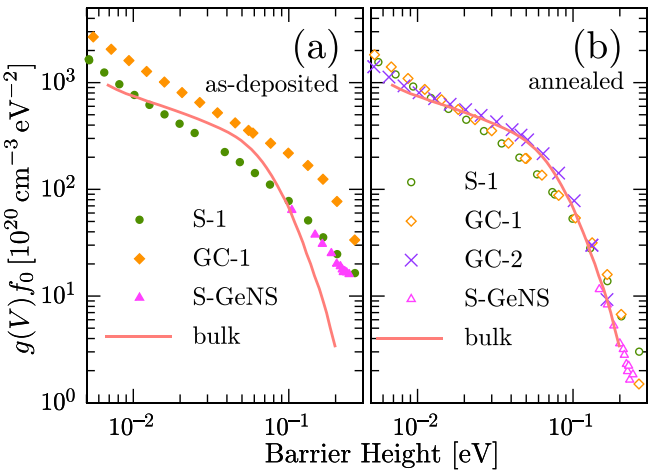

FIG. 6. Barrier Height Distribution for data shown in Fig. 4. Red line is barrier height distribution from Topp and Cahill [51]. (a) As-deposited films. (b) after 36 ks anneal at 500 °C, except GC-2, which was annealed at 900 °C.

As would be expected from the internal friction data, the barrier height distribution for GC-1 is lower in the annealed state than as-deposited over the full range of barrier height energies. For S-1, the as-deposited and annealed distributions have the same value at $V = 0.06$ eV. Below this, the values for the annealed film are approximately 10% higher than for as-deposited. Above, the values for the annealed film are smaller, with the difference growing with increasing energy, to approximately 20% of the as-deposited value at $V = 0.3$ eV. Results for S-2, not shown, are nearly identical to those for S-1. As the barrier height transformation incorporates a frequency dependence, the match between S-1 and S-GeNS is closer than for the internal friction measurements.

IX. SHEAR MODULUS

Shear modulus values are calculated using Eq. (1), with $t_{\text{sub}} = 300$ μm and $G_{\text{sub}} = 62$ GPa for torsion about a Si [110] axis. At low temperatures, the absolute calculated shear modulus values ranged between 28.5 GPa and 30 GPa. However, owing to the ∼5% uncertainty in the film thickness measurements, the uncertainty in 200 nm films was about 1.4 GPa, hence film-to-film comparisons are of little value. Shear modulus values relative to that at low temperatures for each film are shown for S-1, GC-1, and GC-2 in Fig. 7 together with that for bulk silica; the films S-2 and S-3 show the same temperature dependence as S-1 and are not shown in the figure for the sake of clarity. The error bars for $T >$ 100 K represent the uncertainty in the frequency measurements and are different for each particular measurement, and do not include the thickness-related uncertainty. Since the absolute frequency shift upon deposition of a film is proportional to the film thickness but the uncertainties in frequency measurement are independent of film properties, the error bars for the doubly-thick GC-2 are smaller than for the other films [53]. For $T < 100$ K, such error bars are smaller than

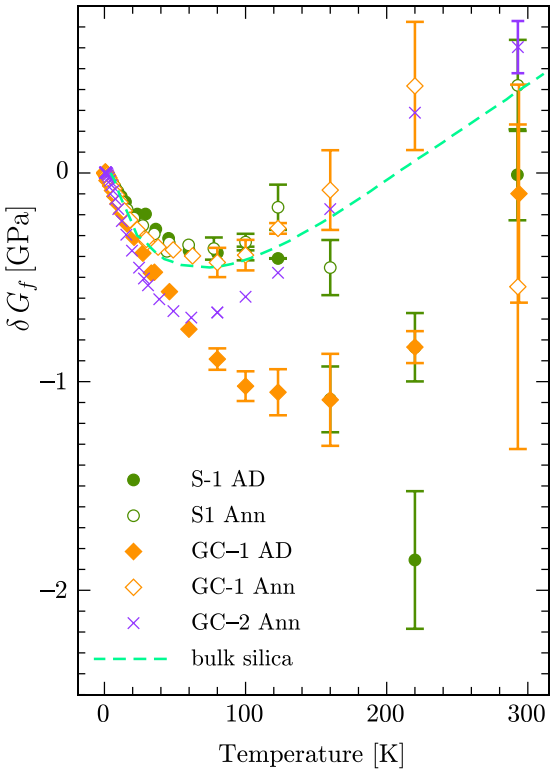

FIG. 7. Relative change in shear modulus of GC-1, S-1, and GC-2 in both as-deposited (AD) and annealed (Ann) states, together with that of bulk silica from McSkimin [52] and Fine [24]. Values measured relative to low-temperature value. The film GC-2 was only measured in the 900 °C-annealed state. Error bars at $T > 100$ K represent error from frequency uncertainties for each measurement. Such error bars below 100 K, and at all temperatures for GC-2 (which is a thicker film), are smaller than the plotted symbols.

the plotted symbols. The room-temperature measurement is subject to the variations in ambient laboratory temperature and although extrapolations of the frequency versus temperature data provide correction, the error bars given represent the possible temperature-induced uncertainty.

The films all show a temperature dependence that follows that of bulk silica [24]: a negative temperature coefficient at the lowest temperatures, switching to a positive temperature coefficient at a temperature at or above 60 K. All the 500 °C-annealed films, and the as-deposited SPECTOR films, follow the temperature dependence of bulk silica at low temperatures, while GC-1 as-deposited and GC-2 annealed-at-900 °C show larger low-temperature changes in shear modulus. The temperature at which the temperature coefficient transitions from negative to positive is at a higher temperature for GC-1 than for any of the other films or for bulk silica. We do not have an explanation for the dramatic apparent drop in the shear modulus calculation for S-1 between 123 K and room temperature but suspect an as-yet unidentified measurement complication.

The changes in shear modulus upon annealing ΔG_{film} are opposite to those of internal friction ΔQ_0^{-1}: While GC-1 shows a decrease in Q_0^{-1} and an increase in G_{film}, the SPECTOR films all show an increase in Q_0^{-1} coupled with a decrease in G_{film}. Values are listed in Table I.

X. MICROSCOPIC MODELS

The calculations by Gilroy and Phillips, and the refinements thereof, do not consider the microscopic origin of the two-state configurations, but such considerations may be of use in understanding why the thin film internal frictions are so different than bulk.

Structurally, bulk silica is composed of a network of tetrahedra with silicon atoms at their centers. The silicon atoms are each bonded to four oxygen atoms, which form the vertices of these tetrahedra, and each oxygen atom is in turn shared by two tetrahedra and bound to two silicon atoms; all the bonds are Si-O. While the tetrahedra are considered mostly rigid, the angle θ of the Si–O–Si bond, and thus of two adjacent tetrahedra, can vary in the range $120^\circ < \theta < 180^\circ$ [54].

The first analysis of the main absorption peak in silica was given by Anderson and Bömmel, who argued that it was the result of a structural relaxation in which oxygen atoms moved laterally across Si–O–Si bonds [55]. Strakna and Savage proposed that some fraction of the Si–O–Si bonds were elongated, creating two equilibrium positions for the oxygen atom [56]. While both of these models, in creating two-state systems, could reproduce the shape of the main absorption peak, Vukcevich pointed out that they would require bond angle distributions that were not consistent with what had been measured [57]. Instead, Vukcevich argued that the main relaxation is rotation of the tetrahedra, which themselves remain otherwise unchanged. Buchenau, Nücker, and Dianoux subsequently modeled coupled rotations of five silica tetrahedra to explain inelastic neutron scattering results [58].

Computer simulations have sought to identify two level systems by looking for configurations that are close in energy with appropriate displacements. Although motivated by the search for two-level tunneling systems, these computations search for the systems via classical, thermally-activated displacements, with the presumption that the same continuum of two-level states explains both the low-temperature anomalies and features such as the main absorption peak. One of the first such computations, using up to 600 atoms, searched the potential energy landscape to find double-well potentials and found that each double-well potential featured displacements of several tetrahedra, a predominant motif of which were chains of several tetrahedra rotating about their edges [59].

The first simulation we are aware of that computed values for internal friction was conducted by Hamdan *et al.* [60] This used a molecular dynamics simulation of 648 atoms run through a series of temperature ramps and quenches. TLSs were identified from atomic displacements, and statistics collected about the TLSs gave numerical $g(V)$ and $f(\Delta)$ curves from which Q^{-1} was calculated. This did reproduce the main absorption peak, although at $Q^{-1} = 1.65 \times 10^{-3}$ near $T = 30$ K it was higher than the $Q^{-1} = 1.0 \times 10^{-3}$ seen in bulk silica. Individual TLSs were typically found to be extended structures involving 20 to 60 atoms, spanning a distance between 10 and 15 Å, with the displacements predominantly rotations of oxygen bonds.

An extension of Hamdan *et al.*'s work by Billman *et al.* computed a two-dimensional correlated distribution $N(V, \Delta)$ of the TLS configurations instead of the separate $g(V)$ and $f(\Delta)$, in part to avoid including the unphysical case of $\Delta \geqslant 2V$, which would be barrier-less [61]. The resulting Q^{-1} calculation did not match as well with the main absorption peak of bulk silica as Hamdan *et al.*'s; the largest peak in this calculation was at 12 K, in line with a peak in IBS silica from Martin *et al.* [which we have plotted in Fig. 5(b), although for a different mode than in Billman *et al.*'s comparison], in addition to other peaks and shoulders. Additionally, the calculation does not show the TLS plateau below 5 K. The Q^{-1} curve features were analyzed as three separate phenomena: the 12 K peak representing $V < 0.04$ eV; a broad peak that could correspond to the main absorption peak with $0.04\,\text{eV} < V < 0.1\,\text{eV}$, and a higher-temperature peak with $0.15\,\text{eV} < V < 0.25\,\text{eV}$.

A more recent computation from Damart and Rodney computed acoustic dissipation in silica directly as a sum over TLSs found in molecular dynamics simulations of 3000 atoms [62]. This computation also did not reproduce the main absorption peak of bulk silica, instead predicting a nonuniform dissipation for $10\,\text{K} < T < 200\,\text{K}$ over which generally $10^{-4} \leqslant Q^{-1} \leqslant 10^{-3}$ but with eight narrow peaks that have not been seen in experiment. The computation also did not have a drop-off in Q^{-1} above the main absorption peak. In general it was found that only ∼6% of the identified TLSs actually contributed substantially to the dissipation, and those that did all fell within the range $|\Delta| < V/3$. This work found three types of TLSs: the first in which a Si atom changes its tetrahedron, with $V > 0.2$ eV; the second in which an oxygen atom changes its coordination, also with high energy barrier; and the third, typically with $V < 0.2$ eV, involving extended structures comprised of three to ten interconnected tetrahedra that rotate. The third type was found to account for most of the dissipation.

The films presented in this paper were vapor deposited onto substrates held far below the glass transition temperature of silica (1200 °C), and as such, in their as-deposited state, may not have the same interconnected distribution of tetrahedra that characterizes bulk fused silica. As seen in Fig. 6, the as-deposited films have an excess of states in the $V > 0.06$ eV range. This corresponds to the energy range of the high-temperature peak in Billman *et al.*'s computations, and these TLSs involve 50 to 100 atoms, with up to 10 oxygen atoms undergoing a coordination change. In Damart and Rodney's analysis, the high-energy-barrier TLSs involve coordination and bond changes. Structures that give rise to these high-energy TLSs may be more prevalent in the unsettled, as-deposited film, while the annealing establishes a more regular network of tetrahedra.

XI. CONCLUSIONS

In contrast to the reproducible internal friction of bulk fused silica, that of thin films is strongly dependent on the deposition method, deposition parameters, and thermal history of the sample. Compared with bulk, as-deposited thin films have a higher internal friction, which indicates, following Eq. (6), either a higher density of two-level tunneling systems $\overline{P}$ or a higher coupling to acoustic phonons γ. Annealing at 500 °C erases many of the differences between the films and is sufficient to induce the steep drop-off of Q^{-1} above the main absorption peak. The main absorption peak itself, however, appears to require exposure to temperatures of at least 900 °C as it is absent or diminished in the thin film samples. The picture that emerges from computational work is that the main absorption peak likely arises from the coordinated rotation of extended structures involving several connected tetrahedra.

ACKNOWLEDGMENTS

The work of T.H.M., X.L., and M.A. was supported by the Office of Naval Research. G.C. and M.G. acknowledge support of the Agence Nationale de la Recherche via Grant No. ANR-18-CE08-0023-03 to their ViSIONs project. We would like to thank Prof. G. Baldi and Prof. F. Hellman for their careful review of an early version of the manuscript. In the document repositories of the LIGO and Virgo Collaborations, this work has numbers LIGO-P2500563 and VIR-0844C-25, respectively.

DATA AVAILABILITY

The data that support the findings of this article are not publicly available upon publication because it is not technically feasible and/or the cost of preparing, depositing, and hosting the data would be prohibitive within the terms of this research project. The data are available from the authors upon reasonable request.

APPENDIX: ELASTIC CONSTANTS AND THE PHONON COUPLING CONSTANT γ

The transformations in Sec. VIII require appropriate values of γ and the elastic modulus. For DPO data, the elastic modulus is the shear modulus. For S-GeNS, finite element modeling shows that the 613 Hz (0,2) mode (no azimuthal and two radial nodes) of the GeNS device is 6.6% bulk deformation and 93.4% shear. Measurements of the silica film deposited on the GeNS device give a Young's modulus of $Y_{\text{GeNS SiO}_2} = 79$ GPa and a Poisson's ratio of $\nu_{\text{GeNS SiO}_2} = 0.23$, which, when combined in the proportion of their deformation energies, give an effective elastic modulus $M_{\text{GeNS SiO}_2} = 33.2$ GPa.

Published values of γ for silica range from 0.4 to 3.0 [63]. The longitudinal γ_l and transverse γ_t values differ: an empirical observation by Berret and Meißner, averaging over 13 different amorphous materials, found $(\gamma_l/\gamma_t)^2 = 2.5$ [64]. The most commonly referred-to values are around 1 eV and are sourced from Doussineau, Matecki, and Schön [65]; however, Van Cleve, Raychaudhuri, and Pohl note that the source data for the γ_t calculation cannot be found in the references [28]. In order to directly compare our measurements with the bulk barrier heights given by Topp and Cahill, we use the same value of $\gamma_t = 0.9$ eV, and use $\gamma_l = \sqrt{2.4}\gamma_t$ [51]. Because the deformation of AS2 of the DPO is almost entirely torsional, γ_t is used, while for the GeNS device, values of γ are combined in proportion to their contribution to the deformation energy, which yields $\gamma_{\text{GeNS SiO}_2} = 1.04\gamma_t = 0.936$ eV.

In the analysis of the barrier height distribution, since we could not determine γ for each film, we assume the same value for all films. Therefore, since the calculation of V in Eq. (9) does not involve γ, the only effect a different value of γ would have would be to shift all the curves together. In this analysis, the relative values between the different films are more important than the absolute value of $g(V)f_0$, and these relative values do not change with different values of γ.

[1] R. O. Pohl, X. Liu, and E. Thompson, Low-temperature thermal conductivity and acoustic attenuation in amorphous solids, Rev. Mod. Phys. **74**, 991 (2002).

[2] X. Liu, B. E. White, Jr., R. O. Pohl, E. Iwanizcko, K. M. Jones, A. H. Mahan, B. N. Nelson, R. S. Crandall, and S. Veprek, Amorphous solid without low energy excitations, Phys. Rev. Lett. **78**, 4418 (1997).

[3] X. Liu, D. R. Queen, T. H. Metcalf, J. E. Karel, and F. Hellman, Hydrogen-free amorphous silicon with no tunneling states, Phys. Rev. Lett. **113**, 025503 (2014).

[4] S. F. Swallen, K. L. Kearns, M. K. Mapes, Y. S. Kim, R. J. McMahon, M. D. Ediger, T. Wu, L. Yu, and S. Satija, Organic glasses with exceptional thermodynamic and kinetic stability, Science **315**, 353 (2007).

[5] K. L. Kearns, S. F. Swallen, M. D. Ediger, T. Wu, Y. Sun, and L. Yu, Hiking down the energy landscape: Progress toward the Kauzmann temperature via vapor deposition, J. Phys. Chem. B **112**, 4934 (2008).

[6] P. W. Anderson, B. I. Halperin, and C. M. Varma, Anomalous low-temperature thermal properties of glasses and spin glasses, Philos. Mag. **25**, 1 (1972).

[7] W. A. Phillips, Tunneling states in amorphous solids, J. Low Temp. Phys. **7**, 351 (1972).

[8] J. M. Martinis, K. B. Cooper, R. McDermott, M. Steffen, M. Ansmann, K. D. Osborn, K. Cicak, S. Oh, D. P. Pappas, R. W. Simmonds, and C. C. Yu, Decoherence in Josephson qubits from dielectric loss, Phys. Rev. Lett. **95**, 210503 (2005).

[9] M. Granata, A. Amato, L. Balzarini, M. Canepa, J. Degallaix, D. Forest, V. Dolique, L. Mereni, C. Michel, L. Pinard, *et al.*, Amorphous optical coatings of present gravitational-wave interferometers, Class. Quantum Grav. **37**, 095004 (2020).

[10] E. Cesarini, M. Lorenzini, E. Campagna, F. Martelli, F. Piergiovanni, F. Vetrano, G. Losurdo, and G. Cagnoli, A "gentle" nodal suspension for measurements of the acoustic attenuation in materials, Rev. Sci. Instrum. **80**, 053904 (2009).

[11] M. Granata, L. Balzarini, J. Degallaix, V. Dolique, R. Flaminio, D. Forest, D. Hofman, C. Michel, R. Pedurand, L. Pinard, *et al.*, Internal friction and Young's modulus measurements on SiO_2 and Ta_2O_5 films done with an ultra-high Q silicon-wafer suspension, Arch. Metall. Mater. **60**, 365 (2015).

[12] T. H. Metcalf, X. Liu, and M. R. Abernathy, Improving the mechanical quality factor of ultra-low-loss silicon resonators, J. Appl. Phys. **123**, 235105 (2018).

[13] K. Sato, M. Shikida, Y. Matsushima, T. Yamashiro, K. Asaumi, Y. Iriye, and M. Yamamoto, Characterization of orientation-dependent etching properties of single-crystal silicon: Effects of KOH concentration, *Tenth IEEE International Workshop on Micro Electro Mechanical Systems*, Sens. Actuators, A **64**, 87 (1998).

[14] M. Shikida, K.-i. Nanbara, T. Koizumi, H. Sasaki, M. Odagaki, K. Sato, M. Ando, S. Furuta, and K. Asaumi, A model explaining mask-corner undercut phenomena in anisotropic silicon etching: A saddle point in the etching-rate diagram, Sens. Actuators, A **97–98**, 758 (2002).

[15] C. L. Spiel, R. O. Pohl, and A. T. Zehnder, Normal modes of a Si(100) double-paddle oscillator, Rev. Sci. Instrum. **72**, 1482 (2001).

[16] X. Liu, S. F. Morse, J. F. Vignola, D. M. Photiadis, A. Sarkissian, M. H. Marcus, and B. H. Houston, On the modes and loss mechanisms of a high Q mechanical oscillator, Appl. Phys. Lett. **78**, 1346 (2001).

[17] SX AR-PC 5000/40, Allresist, https://www.allresist.com/.

[18] B. S. Berry and W. C. Pritchet, Vibrating reed internal-friction apparatus for films and foils, IBM J. Res. Dev. **19**, 334 (1975).

[19] T. Li, F. A. Aguilar Sandoval, M. Geitner, L. Bellon, G. Cagnoli, J. Degallaix, V. Dolique, R. Flaminio, D. Forest, M. Granata, C. Michel, N. Morgado, and L. Pinard, Measurements of mechanical thermal noise and energy dissipation in optical dielectric coatings, Phys. Rev. D **89**, 092004 (2014).

[20] M. Granata, A. Amato, M. Bischi, M. Bazzan, G. Cagnoli, M. Canepa, M. Chicoine, A. Di Michele, G. Favaro, D. Forest, G. M. Guidi, G. Maggioni, F. Martelli, M. Menotta, M. Montani, F. Piergiovanni, and F. Schiettekatte, Optical and mechanical properties of ion-beam-sputtered MgF_2 thin films for gravitational-wave interferometers, Phys. Rev. Appl. **17**, 034058 (2022).

[21] D. M. Photiadis, B. H. Houston, X. Liu, J. A. Bucaro, and M. H. Marcus, Thermoelastic loss observed in a high Q mechanical oscillator, Physica B **316–317**, 408 (2002).

[22] B. E. Deal and A. S. Grove, General relationship for the thermal oxidation of silicon, J. Appl. Phys. **36**, 3770 (1965).

[23] J. W. Marx and J. M. Sivertsen, Temperature dependence of the elastic moduli and internal friction of silica and glass, J. Appl. Phys. **24**, 81 (1953).

[24] M. E. Fine, H. Van Duyne, and N. T. Kenney, Low-temperature internal friction and elasticity effects in vitreous silica, J. Appl. Phys. **25**, 402 (1954).

[25] W. W. Scott and R. K. MacCrone, Anelastic and dielectric relaxation of excess vibrational modes in silica, Phys. Rev. B **1**, 3515 (1970).

[26] K. S. Gilroy and W. A. Phillips, An asymmetric double-well potential model for structural relaxation processes in amorphous materials, Philos. Mag. B **43**, 735 (1981).

[27] A. K. Raychaudhuri and S. Hunklinger, Low frequency elastic properties of glasses at low temperatures—Implications on the tunneling model, Z. Phys. B **57**, 113 (1984).

[28] J. E. Van Cleve, A. K. Raychaudhuri, and R. O. Pohl, Glasslike elastic properties in the ω-β alloys, Z. Phys. B **93**, 479 (1994).

[29] J. Classen, T. Burkert, C. Enss, and S. Hunklinger, Anomalous frequency dependence of the internal friction of vitreous silica, Phys. Rev. Lett. **84**, 2176 (2000).

[30] G. Weiss, A. Daum, M. Sohn, and J. Arndt, Vibrating reed experiments on compacted vitreous silica, Physica B **219–220**, 290 (1996).

[31] F. Travasso, P. Amico, L. Bosi, F. Cottone, A. Dari, L. Gammaitoni, H. Vocca, and F. Marchesoni, Low-frequency internal friction in silica glass, Europhys. Lett. **80**, 50008 (2007).
[32] F. Travasso, L. Bosi, A. Dari, L. Gammaitoni, H. Vocca, and F. Marchesoni, Low-frequency losses in silica glass at low temperature, Mater. Sci. Eng. A **521–522**, 268 (2009).
[33] R. Keil, G. Kasper, and S. Hunklinger, Distribution of barrier heights in a-SiO_2 and a-Se, J. Non-Cryst. Solids **164–166**, 1183 (1993).
[34] S. Brawer, Low-temperature properties of vitreous silica, Phys. Chem. Glasses **16**, 2 (1975).
[35] D. Tielbürger, R. Merz, R. Ehrenfels, and S. Hunklinger, Thermally activated relaxation processes in vitreous silica: An investigation by Brillouin scattering at high pressures, Phys. Rev. B **45**, 2750 (1992).
[36] See, for example, data in McSkimin [52], Anderson [55], Brawer [34], Vacher [48], and Tielburger [35].
[37] K.-i. Sugino and A. Okazaki, Low-temperature thermal expansion of silicon, Jpn. J. Appl. Phys. **29**, 700 (1990).
[38] L.-C. Kuo, H.-W. Pan, C.-L. Chang, and S. Chao, Low cryogenic mechanical loss composite silica thin film for low thermal noise dielectric mirror coatings, Opt. Lett. **44**, 247 (2019).
[39] B. E. White, Jr. and R. O. Pohl, Internal friction of subnanometer $a-SiO_2$ films, Phys. Rev. Lett. **75**, 4437 (1995).
[40] B. E. White, Jr., Elastic properties of amorphous thin films, Ph.D. thesis, Cornell University, 1996.
[41] I. W. Martin, R. Nawrodt, K. Craig, C. Schwarz, R. Bassiri, G. Harry, J. Hough, S. Penn, S. Reid, R. Robie, and S. Rowan, Low temperature mechanical dissipation of an ion-beam sputtered silica film, Class. Quantum Grav. **31**, 035019 (2014).
[42] A. Paolone, E. Placidi, E. Stellino, M. G. Betti, E. Majorana, C. Mariani, A. Nucara, O. Palumbo, P. Postorino, M. Sbroscia, *et al.*, Argon and other defects in amorphous SiO_2 coatings for gravitational-wave detectors, Coatings **12**, 1001 (2022).
[43] X. Liu, E. Iwaniczko, R. O. Pohl, and R. S. Crandall, Molecular hydrogen in hot-wire hydrogenated amorphous silicon, MRS Proc. **507**, 595 (1998).
[44] T. H. Metcalf, Internal friction of solid neon and argon films, Mater. Sci. Eng. A **370**, 150 (2004).
[45] A. V. Leont'eva, G. A. Marinin, and I. A. Oberemchenko, Low temperature internal friction in crystalline argon, Sov. J. Low Temp. Phys. **10**, 671 (1984).
[46] R. Zeller and R. Pohl, Thermal conductivity and specific heat of noncrystalline solids, Phys. Rev. B **4**, 2029 (1971).
[47] J. Jäckle, On the ultrasonic attenuation in glasses at low temperatures, Z. Phys. **257**, 212 (1972).
[48] R. Vacher, J. Pelous, F. Plicque, and A. Zarembowitch, Ultrasonic and Brillouin scattering study of the elastic properties of vitreous silica between 10 and 300 K, J. Non-Cryst. Solids **45**, 397 (1981).
[49] J. Bonnet, On the thermally activated structural relaxation in glasses, J. Non-Cryst. Solids **127**, 227 (1991).
[50] R. Vacher, E. Courtens, and M. Foret, Anharmonic versus relaxational sound damping in glasses. II. Vitreous silica, Phys. Rev. B **72**, 214205 (2005).
[51] K. A. Topp and D. G. Cahill, Elastic properties of several amorphous solids and disordered crystals below 100 K, Z. Phys. B **101**, 235 (1996).
[52] H. J. McSkimin, Measurement of elastic constants at low temperatures by means of ultrasonic waves—Data for silicon and germanium single crystals, and for fused silica, J. Appl. Phys. **24**, 988 (1953).
[53] There are compounded challenges with frequency measurements in the $T > 100$ K temperature range. The change with temperature of the frequency of a DPO is large; the total frequency change upon cooling from room temperature to 77 K is about -29 Hz, an order of magnitude larger than the 3 Hz change from the deposition of a film. Further, the cryostat in which these measurements were made is not designed for this temperature range and frequency equilibration times are long; if measurements are made too hastily then frequency measurements will have large errors.
[54] R. L. Mozzi and B. E. Warren, The structure of vitreous silica, J. Appl. Crystallogr. **2**, 164 (1969).
[55] O. L. Anderson and H. E. Bömmel, Ultrasonic absorption in fused silica at low temperatures and high frequencies, J. Am. Ceram. Soc. **38**, 125 (1955).
[56] R. E. Strakna and H. T. Savage, Ultrasonic relaxation loss in SiO_2, GeO_2, B_2O_3, and As_2O_3 glass, J. Appl. Phys. **35**, 1445 (1964).
[57] M. Vukcevich, A new interpretation of the anomalous properties of vitreous silica, J. Non-Cryst. Solids **11**, 25 (1972).
[58] U. Buchenau, N. Nücker, and A. J. Dianoux, Neutron scattering study of the low-frequency vibrations in vitreous silica, Phys. Rev. Lett. **53**, 2316 (1984).
[59] J. Reinisch and A. Heuer, What is moving in silica at 1 K? A computer study of the low-temperature anomalies, Phys. Rev. Lett. **95**, 155502 (2005).
[60] R. Hamdan, J. P. Trinastic, and H. P. Cheng, Molecular dynamics study of the mechanical loss in amorphous pure and doped silica, J. Chem. Phys. **141**, 054501 (2014).
[61] C. R. Billman, J. P. Trinastic, D. J. Davis, R. Hamdan, and H.-P. Cheng, Origin of the second peak in the mechanical loss function of amorphous silica, Phys. Rev. B **95**, 014109 (2017).
[62] T. Damart and D. Rodney, Atomistic study of two-level systems in amorphous silica, Phys. Rev. B **97**, 014201 (2018).
[63] S. Hunklinger and W. Arnold, Ultrasonic properties of glasses at low temperatures, in *Physical Acoustics: Principles and Methods*, edited by W. P. Mason and R. Thurston (Academic Press, New York, 1976), Vol. 12, pp. 155–215.
[64] J. F. Berret and M. Meißner, How universal are the low temperature acoustic properties of glasses? Z. Phys. B **70**, 65 (1988).
[65] P. Doussineau, M. Matecki, and W. Schön, Connection between the low temperature acoustic properties and the glass transition temperature of fluoride glasses, J. Phys. France **44**, 101 (1983).